Supplement to "Predictability of mean summertime diurnal winds over ungauged mountain glaciers"

J Krishnanand[1], Argha Banerjee[1], R. Shankar[2], Himanshu Kaushik[3], Mohd. Farooq Azam[3], and Chandan Sarangi[4]

[1]Earth and Climate Science, Indian Institute of Science Education and Research Pune, Maharashtra, India
[2]The Institute of Mathematical Sciences, Chennai, Tamil Nadu, India
[3]Department of Civil Engineering, Indian Institute of Technology Indore, Madhya Pradesh, India
[4]Department of Civil Engineering, Indian Institute of Technology Madras, Tamil Nadu, India

Correspondence: Argha Banerjee (argha@iiserpune.ac.in)

Text S1. Relationship between Eq. 1 and linear response

We define the Fourier transform of a time-domain function $f(t)$ as:

$$\hat{f}(\omega) = \int_{-\infty}^{\infty} f(t) e^{i\omega t} dt. \tag{S1}$$

The linear-response model, which assumes that the variation in glacier wind speed is a linear response to the diurnal variation of temperature, is given by:

$$u_d + \tau_0 \frac{d}{dt} u_d = s T_d. \tag{S2}$$

While the present empirical model (Eq. 1) assumes the following relation:

$$u_d + s\tau \frac{d}{dt} T_d = s T_d. \tag{S3}$$

The symbols s_0 and τ_0 above denote the sensitivity of the wind to temperature forcing and the response time, respectively, for the linear-response model. Note that these two parameters are in general different from the corresponding sensitivity s and response time τ in the empirical model, in general. Taking Fourier transform on both sides of this equation (Eq. S2), we obtain:

$$(1 - i\omega\tau_0)\hat{u}_d = s_0 \hat{T}_d \tag{S4}$$

$$\implies \hat{u}_d = \frac{s_0}{(1 - i\omega\tau_0)} \hat{T}_d. \tag{S5}$$

$$\implies \hat{u}_d = \frac{s_0}{(1 + \omega^2\tau_0^2)} (1 + i\omega\tau_0) \hat{T}_d. \tag{S6}$$

In the limit of $\omega^2\tau_0^2 << 1$, this form is similar to the one obtained by taking Fourier transform on both sides of equation S3):

$$\hat{u}_d = s(1 + i\omega\tau)\hat{T}_d. \tag{S7}$$

For the mean hourly summer temperature and wind speed considered here, the dominant frequency is $\omega = 2\pi/24$ hours. Given that the response time $\tau \approx 1$ hr, we are in this low-frequency limit. Thus, for the problem of mean diurnal variability of wind speed addressed here, our empirical model (Equation S4) is equivalent to the linear response model (Eq. S3).

Text S2. Top three multilinear regressions for predicting model parameters s, τ, and $\bar{u}$

As discussed in Sect. 5.2, the top three best performing multilinear regressions to obtain the model parameters are as follows:

The best model with RMSE = 0.686 ms^{-1}:

$$\bar{u} = (2.50 \pm 0.51) + (4.52 \pm 0.80) \times 10^{-3} R_1 - (1.57 \pm 0.25) \times 10^{-3} R_5 + (0.11 \pm 0.02)\mathrm{AR}_{\sigma,1} \tag{S8}$$

$$s = (0.13 \pm 0.09) - (1.69 \pm 0.54) \times 10^{-4} Z_s + (2.17 \pm 0.60) \times 10^{-4} \bar{Z}_{10} \tag{S9}$$

$$\tau = (0.73 \pm 0.49) + (1.93 \pm 1.45) S_{0.1} \tag{S10}$$

$$\tag{S11}$$

The second-best model with RMSE = 0.687 ms^{-1}:

$$\bar{u} = (2.50 \pm 0.51) + (4.52 \pm 0.80) \times 10^{-3} R_1 - (1.57 \pm 0.25) \times 10^{-3} R_5 + (0.11 \pm 0.02)\mathrm{AR}_{\sigma,1} \tag{S12}$$

$$s = (0.13 \pm 0.09) - (1.69 \pm 0.54) \times 10^{-4} Z_s + (2.17 \pm 0.60) \times 10^{-4} \bar{Z}_{10} \tag{S13}$$

$$\tau = (1.95 \pm 0.77) - (1.46 \pm 1.54) \times 10^{-3} \sigma_5 \tag{S14}$$

$$\tag{S15}$$

The third-best model with RMSE = 0.690 ms^{-1}:

$$\bar{u} = (2.50 \pm 0.51) + (4.52 \pm 0.80) \times 10^{-3} R_1 - (1.57 \pm 0.25) \times 10^{-3} R_5 + (0.11 \pm 0.02)\mathrm{AR}_{\sigma,1} \tag{S16}$$

$$s = (0.13 \pm 0.09) - (1.69 \pm 0.54) \times 10^{-4} Z_s + (2.17 \pm 0.60) \times 10^{-4} \bar{Z}_{10} \tag{S17}$$

$$\tau = (1.36 \pm 0.47) - (0.01 \pm 0.03) L \tag{S18}$$

$$\tag{S19}$$

The static variables used in the above equations are described in Supplementary Table S2. Eqs. S10–S12 above is the same Eqs. 7–9 in the main text. Note that no climatic variable appear among the predictors in the top 10 models.

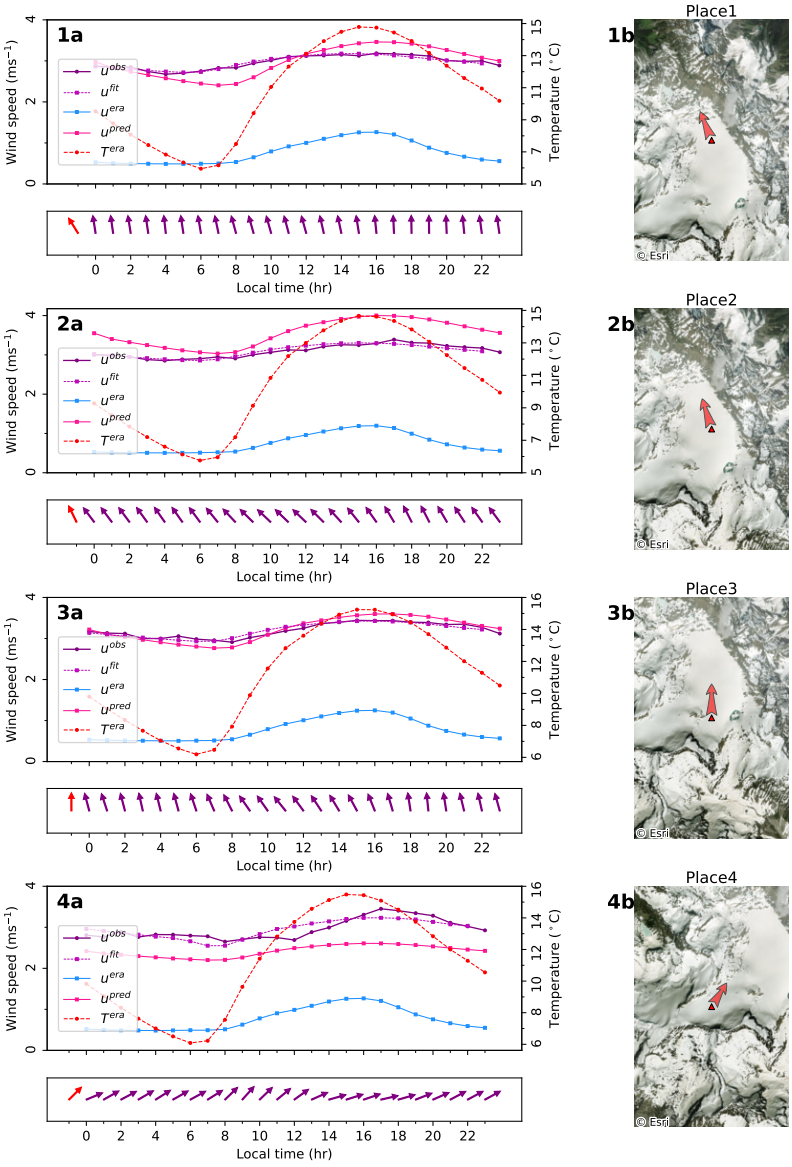

Supplementary Figure S1 . Comparison of model predictions with observations for each of the 28 stations. a) Here u^{obs} denotes the mean hourly values of observed wind speed, u^{fit} denotes the result of fitting Eq. 1 to observations, T^{era} is the ERA5L temperature, u_{pred} denotes the wind speeds predicted using Eqs. 1, 7–9, and ERA5L derived 10m-winds are shown as u^{era}. The purple arrows in the panel below denote the hourly averaged wind vectors for the station, with wind blowing to the north being denoted by an upward arrow. Arrow lengths were rescaled separately for each station so that variations across hours are visible; thus, their lengths are not comparable between stations. The red arrow denotes down-glacier direction which was determined visually from Google Earth. b) The location of weather station (red triangle) on an image of the glacier. The red arrow denotes the down valley direction, which was determined manually. Image Source: Esri, i-cubed, USDA, USGS, AEX, GeoEye, Getmapping, Aerogrid, IGN, IGP, UPR-EGP, and the GIS User Community.

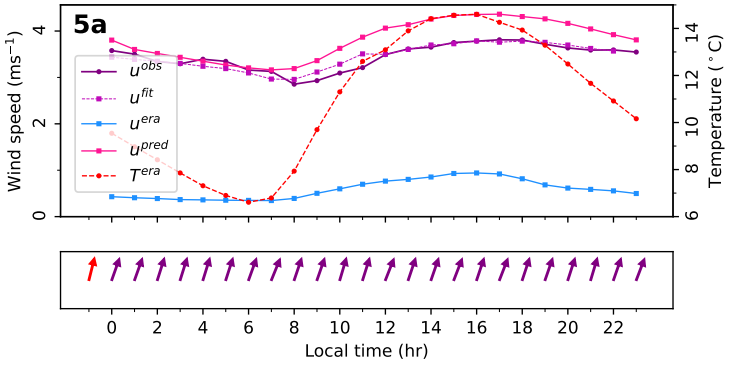
5a
Wind speed (ms^{-1})
Temperature (˚C)
u^{obs}
u^{fit}
u^{era}
u^{pred}
T^{era}
Local time (hr)


Weart1
5b
© Esri

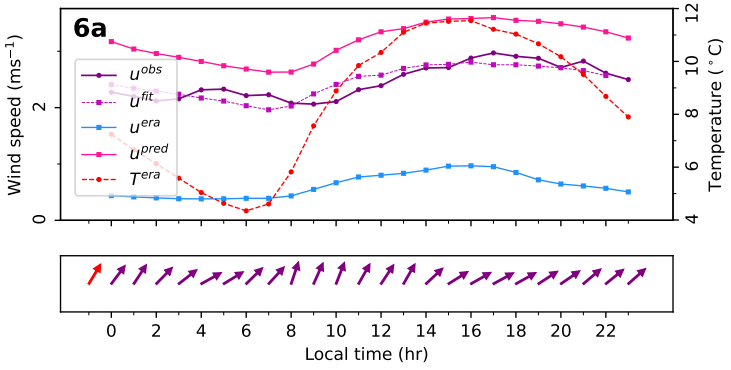
6a
Wind speed (ms^{-1})
Temperature (˚C)
u^{obs}
u^{fit}
u^{era}
u^{pred}
T^{era}
Local time (hr)


Weart2
6b
© Esri

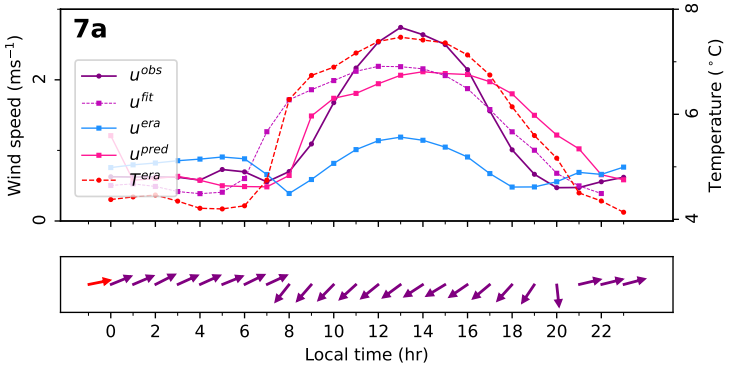
7a
Wind speed (ms^{-1})
Temperature (˚C)
u^{obs}
u^{fit}
u^{era}
u^{pred}
T^{era}
Local time (hr)

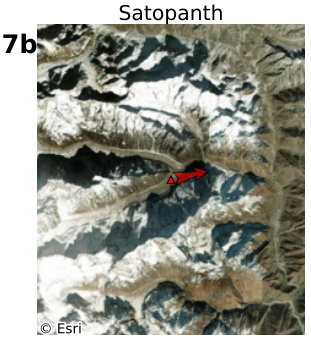
Satopanth
7b
© Esri

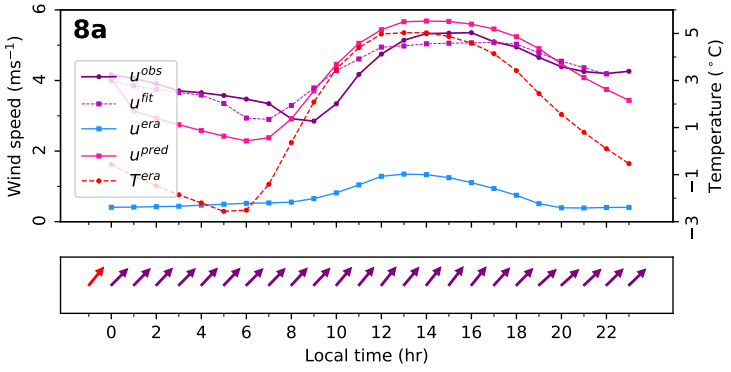
8a
Wind speed (ms^{-1})
Temperature (˚C)
u^{obs}
u^{fit}
u^{era}
u^{pred}
T^{era}
Local time (hr)

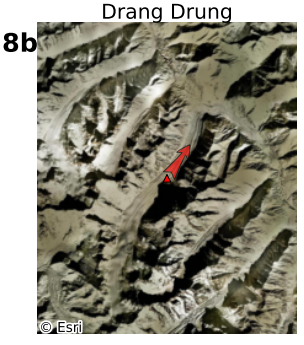
Drang Drung
8b
© Esri

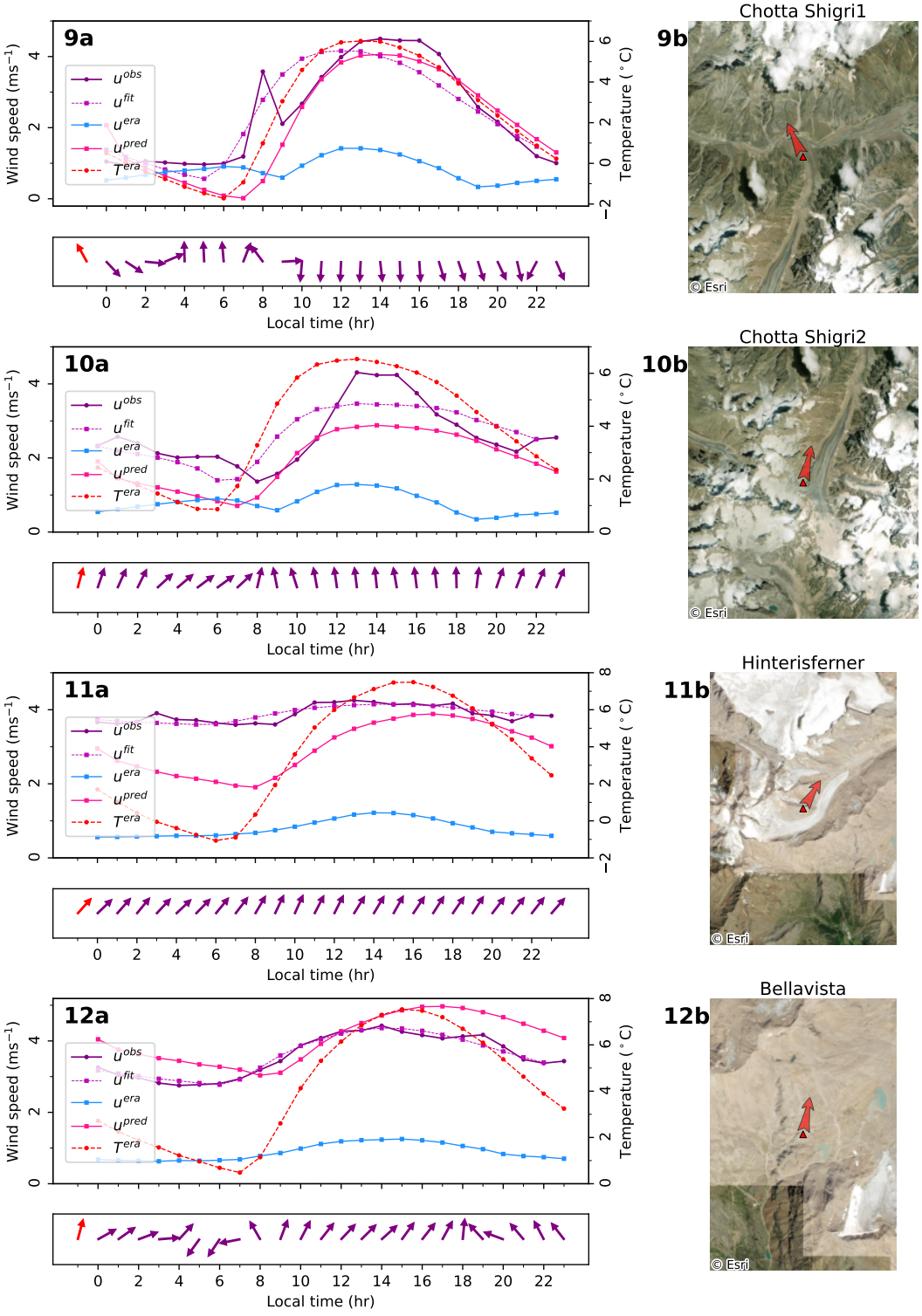
9a
9b
Chotta Shigri1
10a
10b
Chotta Shigri2
11a
11b
Hinterisferner
12a
12b
Bellavista
Wind speed (ms^{-1})
Temperature (˚C)
Local time (hr)
u^{obs}
u^{fit}
u^{era}
u^{pred}
T^{era}
© Esri

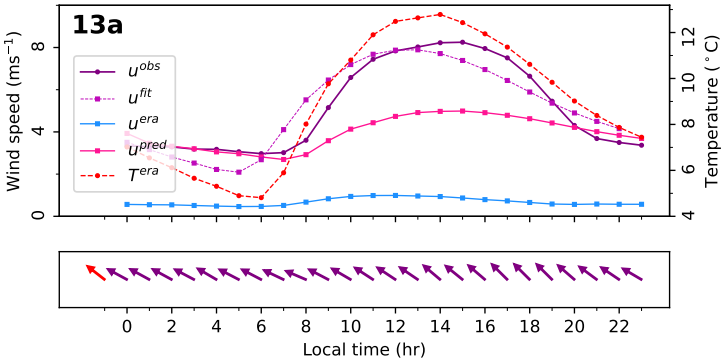

Djankuat

13b

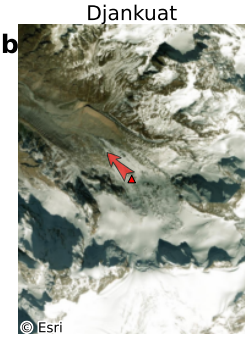

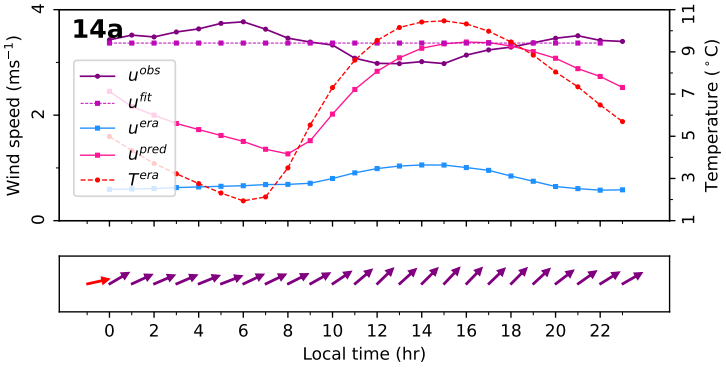

Langenferner

14b

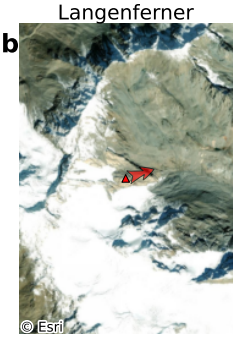

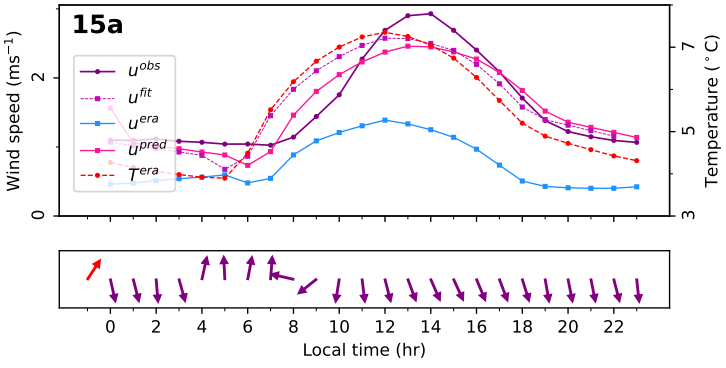

Trakarding

15b

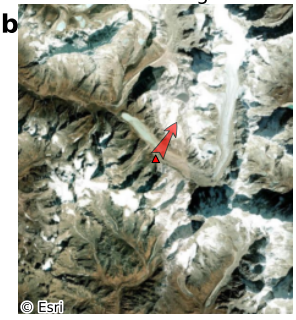

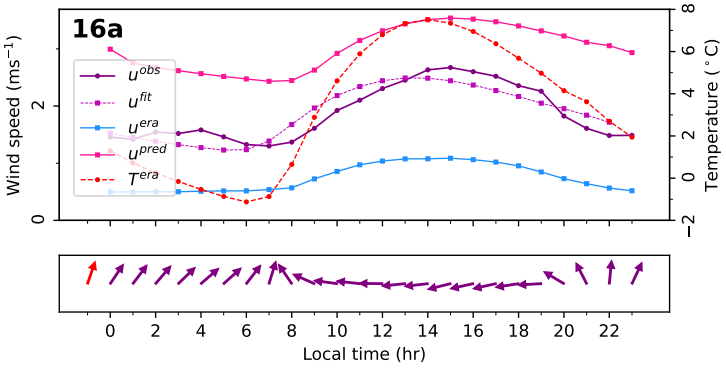

Weissee

16b

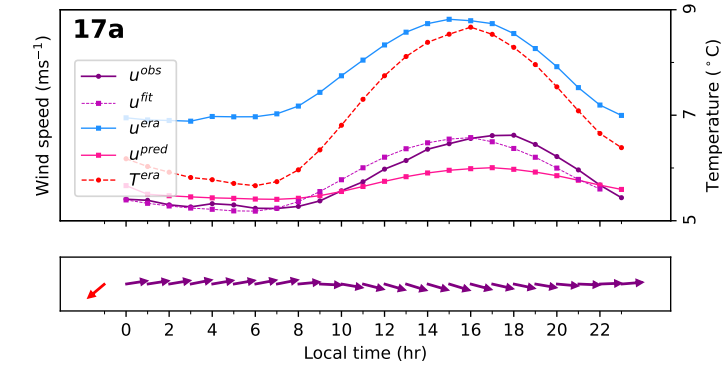

Schiaparelli

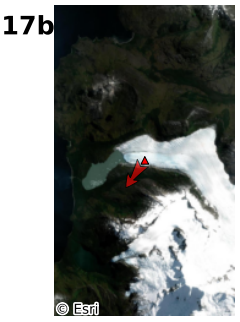

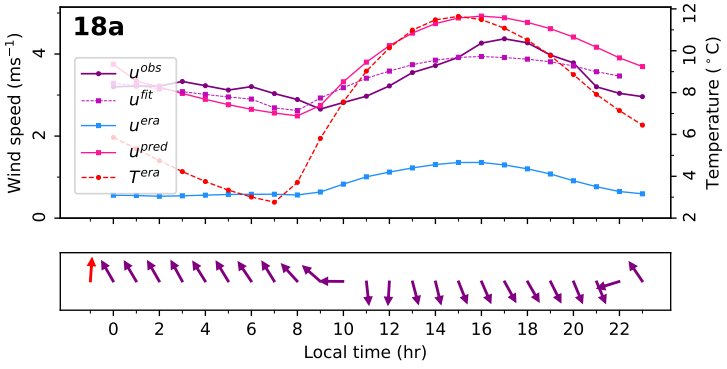

Arolla

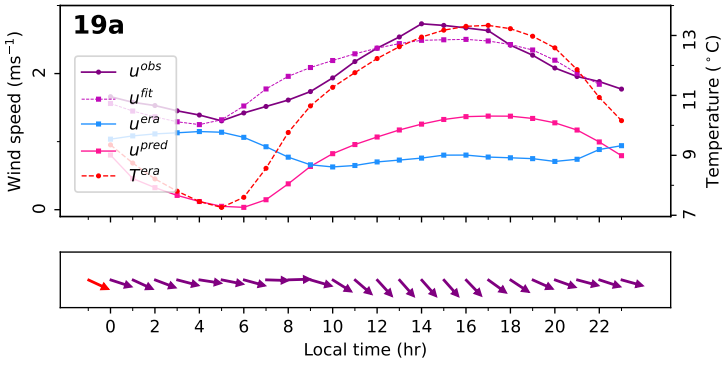

Kennikot

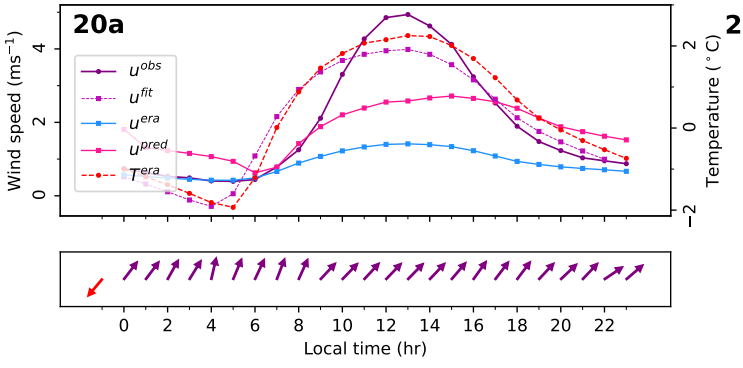

Kalapathar

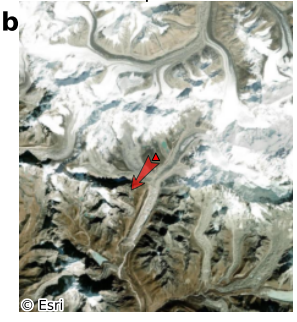

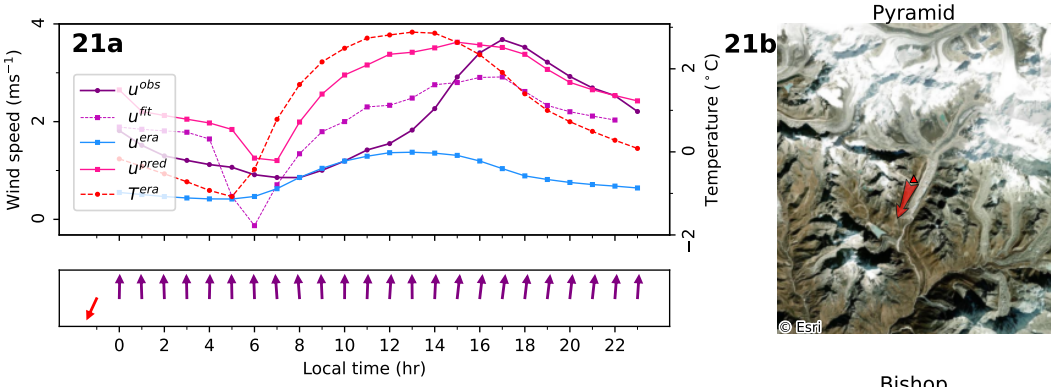

Pyramid

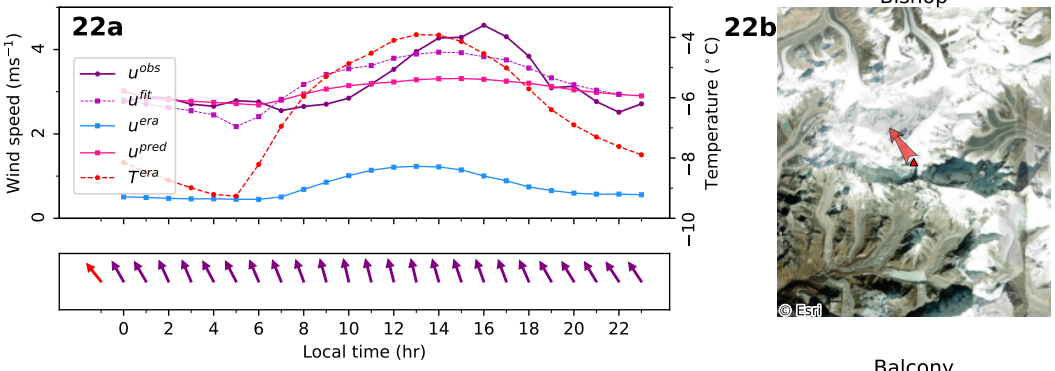

Bishop

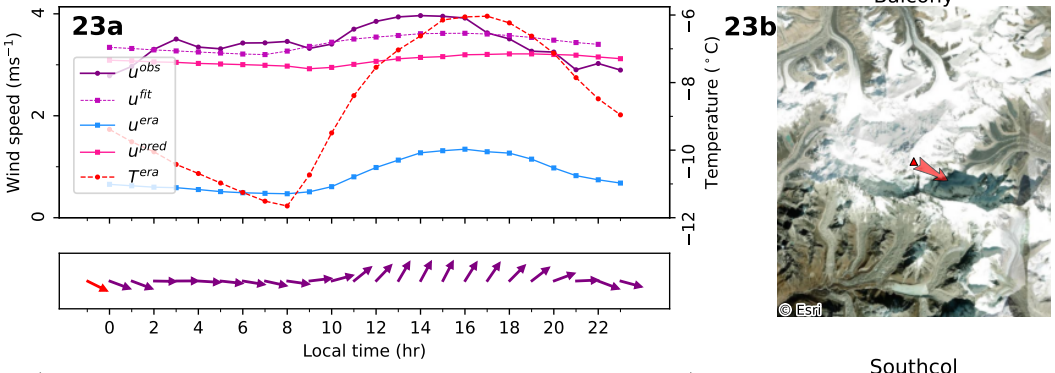

Balcony

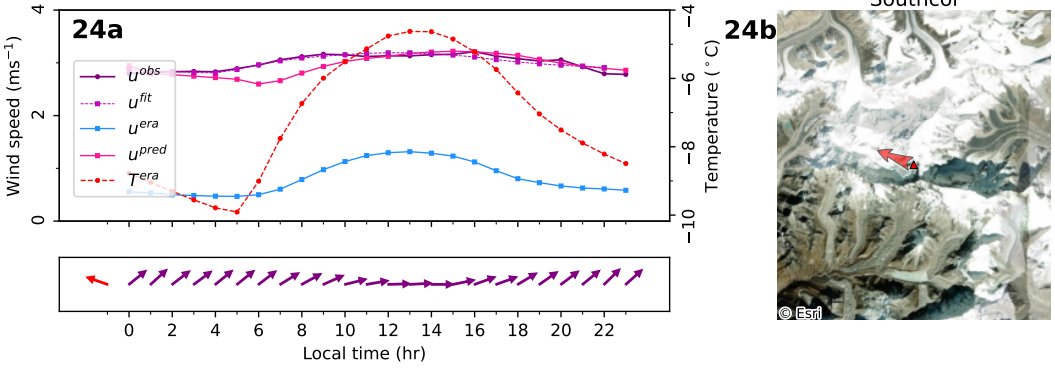

Southcol

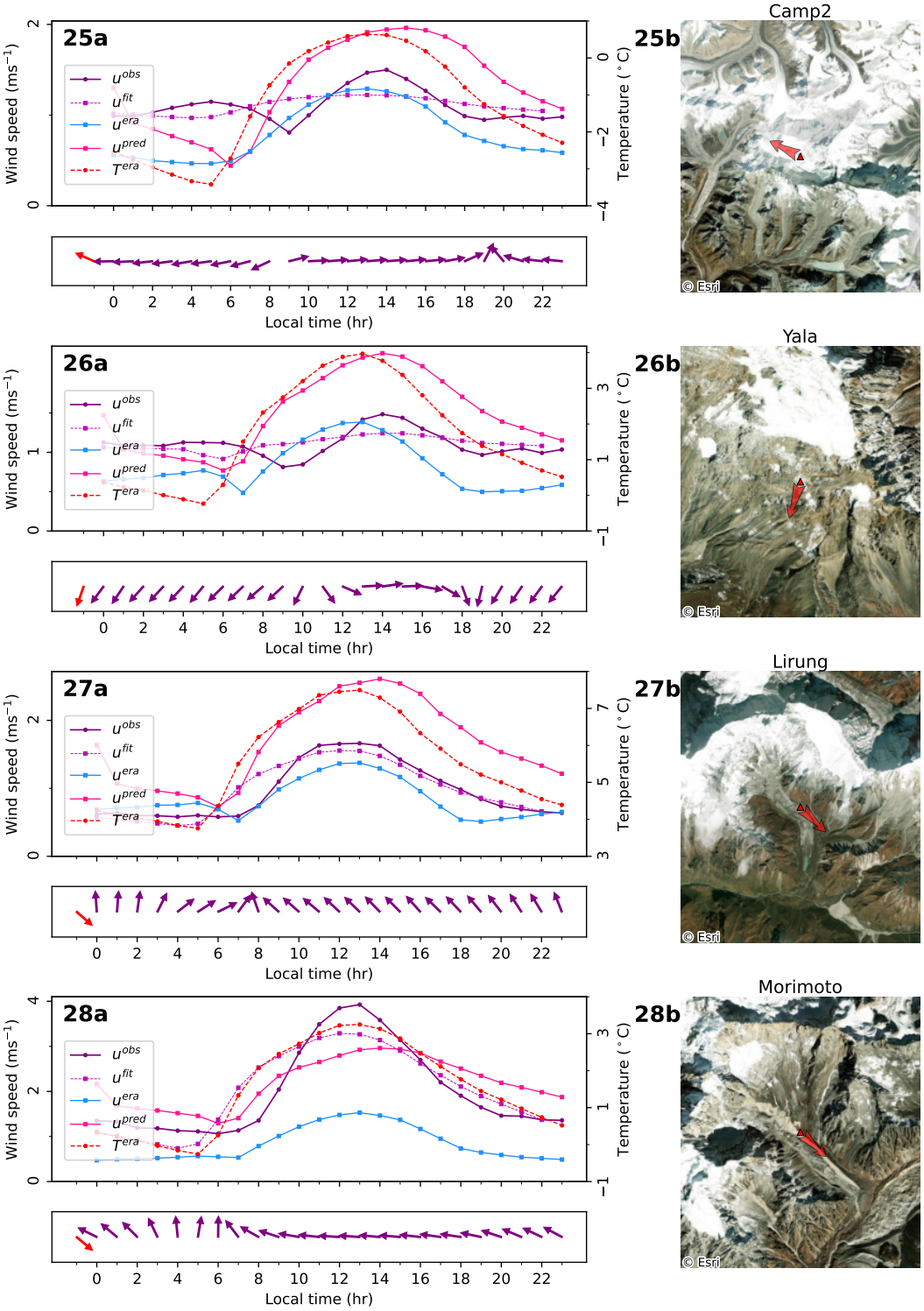
25a
Wind speed (ms^{-1})
Temperature ($^\circ$C)
u^{obs}
u^{fit}
u^{era}
u^{pred}
T^{era}
Local time (hr)
Camp2
25b
© Esri
26a
Wind speed (ms^{-1})
Temperature ($^\circ$C)
Local time (hr)
Yala
26b
© Esri
27a
Wind speed (ms^{-1})
Temperature ($^\circ$C)
Local time (hr)
Lirung
27b
© Esri
28a
Wind speed (ms^{-1})
Temperature ($^\circ$C)
Local time (hr)
Morimoto
28b
© Esri

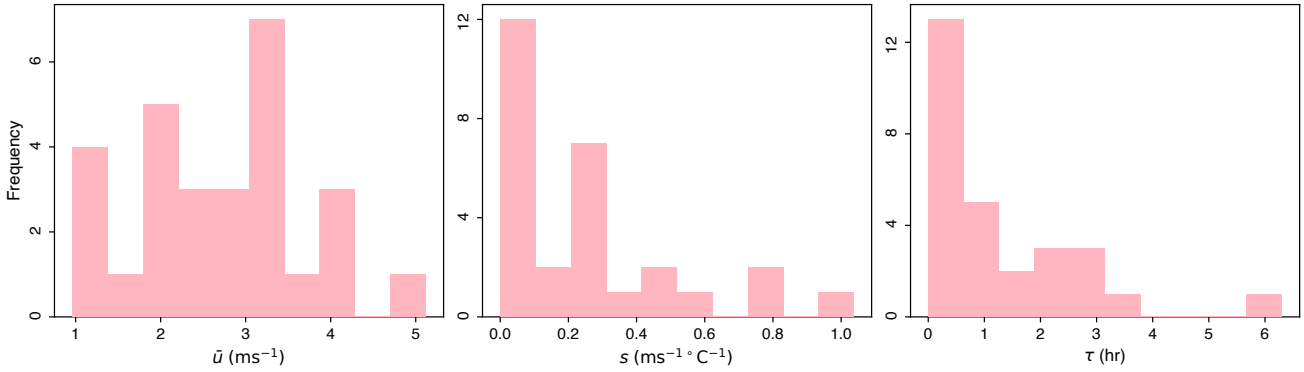

Supplementary Figure S2 . Distribution of model parameters mean wind speed $\overline{u}$, sensitivity of wind speed variation to temperature s and response time τ obtained through fitting Eq. 1 to observations in all 28 stations (main text, section 3.2.1).

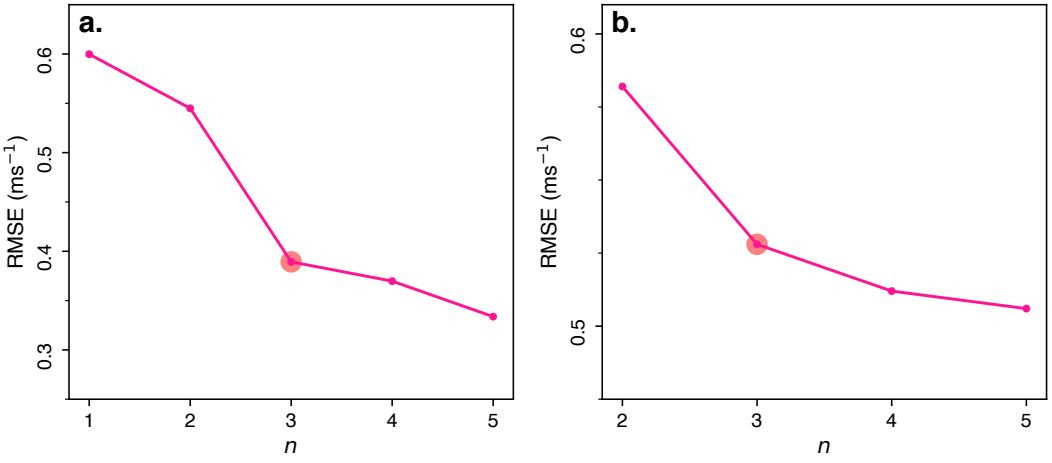

Supplementary Figure S3 . Determination of the optimal number of static variables used in Eqs. 2–4 (main text, section 3.2.2): a) The RMSE of $\bar{u}$ prediction (Eq. 2) for the best n-variable regression model shows that the improvement at 2→3 is larger than that at 3→4. Therefore a $n = 3$ (highlighted with a bigger red circle) model was chosen. b) The RMSE of u_d prediction (Eqs. 2–3) for the best n-variable regression model also led to a $n = 3$ model, following the same criterion.

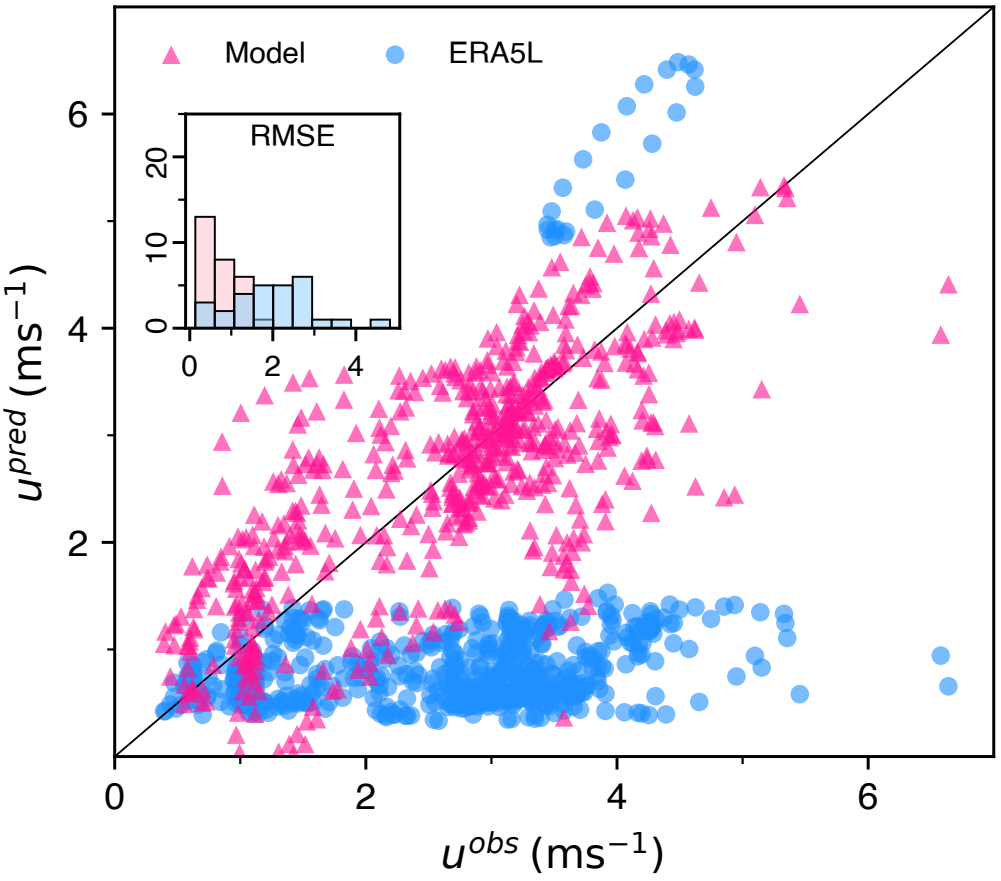

Supplementary Figure S4 . (a) The result of LOOCV (main text, section 4.2.2): For each of the 28 left-out stations, the predicted u is compared to the corresponding observed values. The ERA5L wind speeds for the left-out stations are also shown (blue solid circles). The inset shows the distribution of the 28 RMSEs of the wind speeds predicted for the left-out station by the calibrated model (shown as light pink histogram) and ERA5 (shown as light blue histogram).

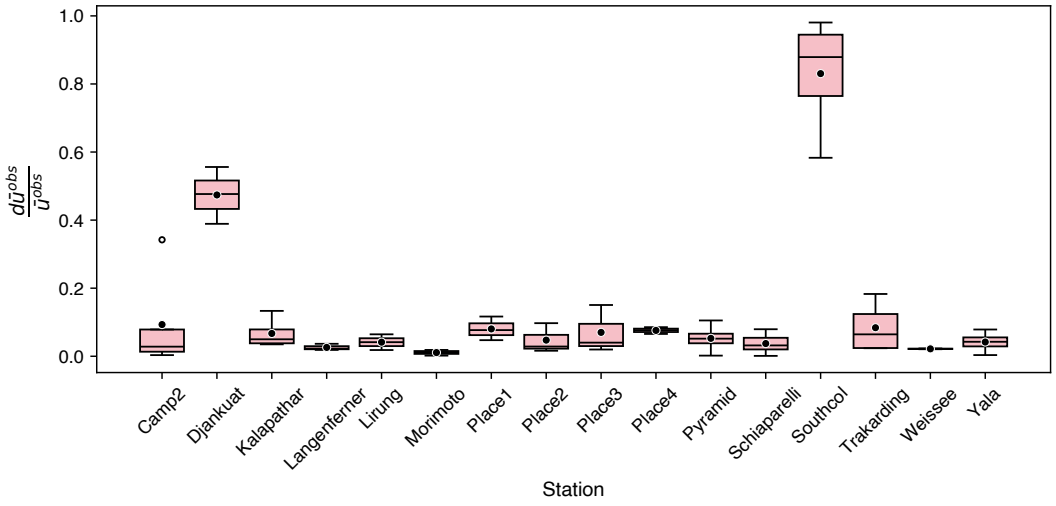

Supplementary Figure S5 . For the stations with more than one year of data, the box-plot shows the distribution of fractional absolute deviations $d\bar{u}/\bar{u}$ across different years. South Col station has the highest inter-annual mean wind speed variability. This is one among the three high-altitude stations (Balcony and Bishop are the other two) located near Mt. Everest, with possible influence of synoptic scale winds. Djankuat Glacier station, second among the two stations with the most inter-annual variability of mean wind speed, also has the highest observed mean wind speed among all stations. The winds in this station is predominantly katabatic. Djankuat is also the glacier with the largest inter-annual observed mean temperature variability.

Supplementary Table S1 : Information about glaciers and the weather station datasets used in this work, and the associated glaciers

Station name, Data source	**Station Type**	**Period for which data was available (number of summer days)**	**Latitude, Longitude**	**Elevation (m)**	**Glacier length (km)**	**Glacier area (km^2)**	**Mean temperature (°C)**	**Mean wind (m/s)**	**Glacier type**
Arolla (Shaw, 2023)	On-glacier	2022-07-06 to 2022-09-18 (74 days)	45.97, 7.52	2852	4.4	3.8	7.4	3.4	Debris-free valley glacier
Balcony (Matthews and Coauthors, 2020)	Off-glacier	2019-06-01 to 2019-09-30 (122 days)	27.9826, 86.9292	8323	18.5	26.4	-16.7	3.4	Debris-covered valley glacier
Bellavista (Strasser and Marke, 2017)	Off-glacier	2015-07-27 to 2015-09-28 (64 days)	46.78284, 10.79138	2799	3.2	3.1	4.3	3.6	Debris-free valley glacier
Bishop (Matthews and Coauthors, 2020)	Off-glacier	2022-06-01 to 2022-07-29 (59 days)	27.9735, 86.9308	7857	18.5	26.4	-17.3	3.2	Debris-covered valley glacier
Camp2 (Matthews and Coauthors, 2020)	On-glacier	2019-06-01 to 2023-07-01 (518 days)	27.981, 86.9023	6485	18.5	26.4	-4.0	1.1	Debris-covered valley glacier

Chotta Shigri1 (Mandal et al., 2022)	On-glacier	2022-08-16 to 2022-09-29 (56 days)	32.2858, 77.5305	3844	9.5	16.8	0.0	2.4	Debris-free valley glacier
Chotta Shigri2 (Mandal et al., 2022)	On-glacier	2022-06-07 to 2022-09-29 (86 days)	32.228297, 77.506293	4871	9.5	16.8	2.4	2.6	Debris-free valley glacier
Djankuat (Rets and Popovnin, 2019)	On-glacier	2007-06-17 to 2009-09-30 (231 days)	43.198, 42.757	2976	3.2	3.0	7.0	5.1	Partly debris-covered-valley glacier
Drang Drung (This study)	On-glacier	2023-06-01 to 2023-09-23 (98 days)	33.787596, 76.333945	4601	24.7	68.4	5.5	4.2	Lake-terminating Debris-free valley glacier
Hinterisferner (Stocker-Waldhuber et al., 2013)	Off-glacier	2012-06-01 to 2012-09-30 (121 days)	46.79867, 10.76042	3027	8.5	8.0	4.3	3.9	Debris-free valley glacier
Kalapathar (EvK2CNR station)	Off-glacier	2009-06-01 to 2012-09-30 (457 days)	27.99, 86.83	5600	18.5	26.4	0.1	2.0	Debris-covered valley glacier
Kennikot (Buri et al., 2022)	On-glacier	2019-05-31 to 2019-08-21 (82 days)	61.4841, -142.9283	657	44.9	292.5	10.5	2.0	Debris-covered valley glacier
Langenferner (Galos, 2019)	Off-glacier	2013-06-01 to 2015-08-27 (332 days)	46.47245, 10.61391	2954	2.9	2.2	4.0	3.4	Debris-free valley glacier
Lirung (ICIMOD and Utrecht University, 2020a)	Off-glacier	2018-06-01 to 2019-08-10 (186 days)	28.24, 85.56	4276	8.6	4.8	8.1	1.0	Debris-covered valley glacier
Morimoto (ICIMOD and Utrecht University, 2020b)	Off-glacier	2017-06-01 to 2019-09-30 (365 days)	28.25296, 85.68152	4925	4.6	1.4	3.4	2.0	Debris-covered valley glacier
Place1 (Shea, 2010)	On-glacier	2006-08-04 to 2008-08-12 (206 days)	50.426073, -122.601628	1970	3.8	3.0	4.7	3.0	Debris-free valley glacier
Place2 (Shea, 2010)	On-glacier	2006-08-04 to 2008-09-28 (266 days)	50.421835, -122.598482	2025	3.8	3.0	4.5	3.1	Debris-free valley glacier
Place3 (Shea, 2010)	On-glacier	2006-08-04 to 2008-08-31 (241 days)	50.414718, -122.600217	2095	3.8	3.0	5.2	3.2	Debris-free valley glacier
Place4 (Shea, 2010)	On-glacier	2006-08-04 to 2008-08-25 (189 days)	50.412846 , -122.615898	2330	3.8	3.0	4.3	2.9	Debris-free valley glacier
Pyramid (EvK2CNR station)	Off-glacier	2009-06-01 to 2012-09-29 (473 days)	27.95792, 86.814807	5050	18.5	26.4	2.1	2.0	Debris-covered valley glacier
Satopanth (This study)	On-glacier	2017-06-29 to 2017-09-29 (92 days)	30.773251 , 79.408794	3910	20.1	57.0	9.7	1.2	Debris-covered valley glacier
Schiaparelli (Arigony-Neto et al., 2023)	On-glacier	2016-05-31 to 2020-09-09 (586 days)	-54.4, -70.87	197	10.8	24.8	7.1	3.9	Lake-terminating Debris-free glacier

Southcol (Matthews and Coauthors, 2020)	Off-glacier	2019-06-01 to 2023-07-04 (419 days)	27.9719, 86.9295	7905	18.5	26.4	-13.4	3.07	Debris-covered valley glacier
Trakarding (Fujita, Sunako, Sakai, 2021)	Off-glacier	2016-06-01 to 2019-09-29 (487 days)	27.843, 86.487	4821	17.9	32.1	4.6	1.6	Debris-covered valley glacier
Weart1 (Shea, 2010)	On-glacier	2007-07-10 to 2007-09-06 (58 days)	50.155944, -122.760257	2164	6.5	8.1	4.0	3.5	Debris-free valley glacier
Weart2 (Shea, 2010)	On-glacier	2007-07-10 to 2007-09-06 (58 days)	50.138823, -122.775232	2298	6.5	8.1	4.8	2.5	Debris-free valley glacier
Weissee (Stocker-Waldhuber et al., 2022)	Off-glacier	2017-06-01 to 2018-09-30 (243 days)	46.872909, 10.714437	3507	7.8	16.7	7.5	1.9	Debris-free valley glacier
Yala (ICIMOD, 2016)	Off-glacier	2016-06-01 to 2019-09-30 (464 days)	28.23, 85.62	5214	2.2	2.1	1.2	1.1	Debris-free cirque glacier

Supplementary Table S2 : Description of static variables used in section 3.1.2. Here, ALOS World 3d refers to the 30-m resolution digital elevation model from Tadono et al. (2014), GEE refers to Google Earth Engine (Gorelick et al., 2017), RGI7 refers to the Randolf Glacier Inventory 7 (RGI7.0-Consortium, 2023) and QGIS refers to the Geographic Information System (GIS) application (QGIS Development Team, 2024)

Symbol	**Description**	**Unit**	**Source**
A_g	Area of glacier	km^2	RGI 7
$AR_{\sigma,x}$	The ratio of σ_x to W_c.[1]	unitless	QGIS
$AR_{R,x}$	The ratio of height scale of the valley cross section to its width scale.	unitless	GEE,RGI7, and QGIS
D_c	Perpendicular distance from station to centerline	km	RGI7,QGIS
$\overline{D}_c$	Perpendicular distance from station to centerline, normalised with glacier width at the station location	unitless	RGI7 and QGIS
D_h	Distance from station to higher tip of centerline measured along the centerline	km	RGI7 and QGIS
$\overline{D}_h$	Distance from station to higher tip of centerline measured along the centerline, normalised with glacier length	unitless	RGI7 and QGIS
D_t	Distance from station to lower tip of centerline measured along the centerline	km	RGI7 and QGIS
$\overline{D}_t$	Distance from station to lower tip of centerline measured along the centerline, normalised with glacier length	unitless	RGI7 and QGIS
K	Continentality index, difference between maximum and minimum of monthly averaged temperature	°C	ERA5L

K_C	Latitude corrected continentality index (Conrad, 1946), derived from ERA5 data.	unitless	ERA5L
L	Length of glacier	km	RGI7
R_1	Difference between maximum and minimum elevation inside 1 km circular buffer of station	km	GEE and ALOS World 3D
R_1	Difference between maximum and minimum elevation inside 5 km circular buffer of station	km	GEE and ALOS World 3D
R_5	Difference between maximum and minimum elevation inside 10 km circular buffer of station	km	GEE and ALOS World 3D
R_{10}	Difference between maximum and minimum elevation inside 20 km circular buffer of station	km	GEE and ALOS World 3D
$S_{0.1}$	Slope of 100 m resolution topography at station location	degrees	GEE and ALOS World 3D
S_1	Slope of 1 km resolution topography at station location	degrees	GEE and ALOS World 3D
S_{10}	Slope of 10 km resolution topography at station location	degrees	GEE and ALOS World 3D
S^{rgi}	Slope of glacier	degrees	RGI7
σ_1	Standard deviation of elevations around 1 km square buffer of station	m	GEE and ALOS World 3D
σ_5	Standard deviation of elevations around 10 km circular buffer of station	m	GEE v ALOS World 3D
σ_{10}	Standard deviation of elevations around 100 km circular buffer of station	m	GEE and ALOS World 3D
$\bar{T}^{era}$	Mean summer months (JJAS) temperature of station derived	°C	ERA5L
W_c	Width of glacial valley at the location of station[2]	km	QGIS
$\bar{W}_g$	Mean width of glacier (A_g/L_g)	km	RGI 7
Z_s	Elevation of 30m resolution topography at the station	m	Alos World 3d
$\bar{Z}_{10}$	Mean elevation of 30m resolution topography inside 10 km buffer of station	m	GEE and Alos World 3d
Z_{max}	Maximum elevation of glacier	m	RGI7
Z_{min}	Minimum elevation of glacier	m	RGI7
Z_{range}	$Z_{max} - Z_{min}$	m	RGI7
$\overline{Z}$	Normalized station elevation, defined as $Z_s/(Z_{max} - Z_{min})$	unitless	RGI7 and Weather station metadata

[2]For brevity, the symbol AR has been used in place of $AR_{\sigma,1}$ throughout the main text.

[2]W_c for on-glacier stations, was obtained using QGIS by measuring the width of RGI7 shape-file of the glacier measured perpendicular to the glacier centerline at the station location. For off-glacier stations in de-glaciated valleys, it was defined as the moraine-moraine distance at the station location from Google Earth Imagery, measured perpendicular to the central flow-line of the valley. For all other cases, was taken as $\bar{W}_g$.

Supplementary Table S3 : Details of the best-fit regression model discussed in Section 4.1.2. Values in parentheses denote the uncertainty in the last digits of the corresponding regression coefficients, expressed as their standard errors. For example, 25(5) indicates 25 ± 5. The correlation coefficient column shows the correlation between each model parameter and its associated predictor variable. T-statistics, defined as the ratio between the regression coefficient and its standard error, can be interpreted as the relative importance of a static variable in the multilinear regression.

Model parameter	**Static variable**	**Regression coefficient**	**Correlation coefficient**	**T-statistics**
$\bar{u}$	k	$25(5) \times 10^{-1}$	0.51	4.90
	R_1	$45(8) \times 10^{-4}$	-0.08	5.63
	R_5	$-15(2) \times 10^{-4}$	-0.42	6.20
	AR	$11(2) \times 10^{-2}$	-0.05	5.67
s	k	$13(9) \times 10^{-2}$	0.10	1.41
	Z_s	$-17(5) \times 10^{-5}$	0.11	3.13
	$\bar{Z}_{10}$	$22(6) \times 10^{-5}$	0.32	3.62
τ	k	$73(49) \times 10^{-2}$	0.50	1.49
	$S_{0.1}$	$19(14) \times 10^{-1}$	0.24	1.33

Supplementary Table S4 : For each of the 28 stations, the RMSE between u^{pred} from the calibrated model (Section 4.2.1) and u^{obs} is presented. The RMSEs from the LOOCV model (Section 4.2.2) for the 28 left-out stations are also included, along with the corresponding RMSEs for ERA5L winds for comparison.

Station Name	**RMSE (ms^{-1})**		
	Calibrated Model	**LOOCV Model**	**ERA5L**
Arolla	0.65	0.71	2.55
Balcony	0.48	0.57	2.61
Bellavista	0.62	0.69	2.71
Bishop	0.51	0.59	2.48
Camp2	0.48	0.54	0.38
Chotta Shigri1	0.81	0.85	1.98
Chotta Shigri2	0.84	0.91	1.96
Djankuat	1.84	1.98	4.82
Drang Drung	0.72	0.96	3.55
Hintereisferner	1.07	1.18	3.09

Kalapathar	1.07	1.14	1.64
Kennikot	1.18	1.18	1.26
Langenferner	1.27	1.34	2.63
Lirung	0.75	0.89	0.23
Morimoto	0.58	0.6	1.3
Place1	0.23	0.25	2.2
Place2	0.49	0.54	2.35
Place3	0.12	0.13	2.44
Place4	0.56	0.6	2.21
Pyramid	0.96	1.21	1.41
Satopanth	0.43	0.43	0.77
Schiaparelli	0.27	0.32	1.63
Southcol	0.16	0.18	2.2
Trakarding	0.24	0.25	0.95
Weart1	0.42	0.47	2.87
Weart2	0.73	0.78	1.85
Weisse	1.15	1.26	1.15
Yala	0.57	0.62	0.39

Supplementary Table S5 : Comparison of the turbulent heat flux estimated using the simple bulk-aerodynamic model (Cuffey and Paterson, 2010). . The mean summertime air temperature T^{era} (°C), the dew-point temperature T^{era}_{dew} ((°C), and the surface pressure P (Pa) at each station are obtained from ERA5. The vapor pressure e (Pa) and saturation vapor pressure es (Pa) is calculated with P, Tera and Tdew by using the equation described in (Bolton, 1980; Buck, 1981). Using the methods described in section 2.6, we estimate sensible heat flux Q_{shf} (Wm^{-2}), latent heat flux Q_{lhf}(Wm^{-2}) and the total turbulent heat flux $Q_{thf} = Q_{shf} + Q_{lhf}$ (Wm^{-2}) for each station. The fluxes obtained when the mean wind speed is taken from our model ($\bar{u}^{pred}$), and those obtained directly from ERA5 ($\bar{u}^{era}$), are compared with the same estimated using mean wind speed observed at the station ($\bar{u}^{obs}$).

	Constants derived from ERA5L					**Mean wind speed**			**Sensible heat flux**			**Latent heat flux**			**Turbulent heat flux**		
Name	T^{era}	T^{era}_{dew}	e	e_s	P	$\bar{u}^{obs}$	$\bar{u}^{pred}$	$\bar{u}^{era}$	Q^{obs}_{shf}	Q^{pred}_{shf}	Q^{era}_{shf}	Q^{obs}_{lhf}	Q^{pred}_{lhf}	Q^{era}_{lhf}	Q^{obs}_{thf}	Q^{pred}_{thf}	Q^{era}_{thf}
Arolla	7.4	-0.1	606.2	1026.7	71993.5	3.4	3.8	0.8	46.2	51.3	11.6	-50.9	-56.5	-12.8	-4.7	-5.2	-1.2
Balcony	-8.7	-3.5	471.8	291.3	50300.3	3.4	3.1	0.8	-38.6	-34.9	-9.4	22.1	20.0	5.4	-16.5	-15.0	-4.0
Bellavista	4.1	0.9	650.4	816.8	72869.9	3.6	4.0	0.9	27.3	30.9	6.8	-21.3	-24.1	-5.3	6.0	6.8	1.5
Bishop	-6.5	-3.0	491.7	353.2	50665.5	3.2	3.0	0.7	-27.0	-25.7	-6.3	15.8	15.0	3.7	-11.2	-10.7	-2.6

Camp2	-1.3	-3.2	482.5	550.5	50563.6	1.1	1.3	0.8	-1.8	-2.1	-1.3	-2.7	-3.2	-1.9	-4.5	-5.3	-3.3
Chotta Shigri1	2.3	-0.4	593.4	718.7	58103.9	2.4	2.1	0.8	8.1	7.0	2.8	-10.8	-9.3	-3.7	-2.7	-2.3	-0.9
Chotta Shigri2	3.8	1.0	657.6	803.7	58176.7	2.6	1.9	0.8	15.0	11.0	4.5	-13.7	-10.0	-4.1	1.4	1.0	0.4
Djankuat	8.7	3.0	757.7	1125.6	71659.9	5.1	3.9	0.7	82.4	63.2	11.0	-67.4	-51.7	-9.0	15.0	11.5	2.0
Drang Drung	1.4	-4.3	445.3	675.2	56415.5	4.2	4.1	0.7	8.4	8.1	1.4	-34.6	-33.3	-5.8	-26.2	-25.2	-4.4
Hinterisferner	3.4	0.4	629.7	778.9	72919.5	3.9	3.0	0.8	24.7	18.8	5.1	-20.8	-15.8	-4.3	4.0	3.0	0.8
Kalapathar	0.3	-1.6	542.0	624.3	53165.7	2.0	1.8	0.9	0.8	0.7	0.4	-5.8	-5.3	-2.6	-5.0	-4.6	-2.2
Kennikot	10.7	7.1	1009.0	1287.8	90928.8	2.0	0.8	0.9	49.6	20.2	21.7	-19.7	-8.0	-8.6	29.9	12.2	13.1
Langenferner	6.5	2.5	730.3	971.1	75768.8	3.4	2.5	0.8	43.1	31.4	9.7	-29.0	-21.1	-6.6	14.1	10.2	3.2
Lirung	5.5	1.9	702.7	902.9	55918.3	1.0	1.6	0.8	7.6	13.0	6.6	-6.9	-11.7	-6.0	0.7	1.2	0.6
Morimoto	1.5	-0.3	598.0	680.7	53513.4	2.0	2.2	0.8	4.1	4.5	1.7	-5.9	-6.4	-2.5	-1.8	-2.0	-0.8
Place1	10.7	4.7	852.8	1287.6	87208.1	3.0	3.0	0.8	71.5	71.7	18.5	-46.2	-46.3	-12.0	25.3	25.4	6.6
Place2	10.5	5.1	876.2	1272.0	87209.5	3.1	3.6	0.7	73.3	84.1	17.7	-43.9	-50.3	-10.6	29.5	33.8	7.1
Place3	11.1	5.4	895.2	1321.5	87207.7	3.2	3.2	0.8	79.9	80.4	19.2	-48.8	-49.1	-11.8	31.1	31.3	7.5
Place4	11.1	5.3	889.8	1321.3	87216.8	3.0	2.4	0.8	73.8	60.4	19.0	-45.6	-37.4	-11.8	28.1	23.0	7.2
Pyramid	1.0	-1.5	547.2	659.1	53179.8	2.0	2.6	0.9	2.8	3.8	1.2	-7.8	-10.6	-3.4	-5.0	-6.8	-2.2
Satopanth	5.6	0.8	645.3	912.5	57746.3	1.2	1.2	0.8	10.0	10.2	6.7	-11.4	-11.6	-7.6	-1.4	-1.4	-0.9
Schiaparelli	7.0	3.5	783.5	999.3	96673.8	3.9	3.8	5.5	68.0	66.2	95.9	-30.3	-29.5	-42.7	37.7	36.8	53.2
Southcol	-7.2	-3.3	479.7	333.6	50518.7	3.0	2.9	0.8	-28.1	-27.5	-7.6	15.7	15.4	4.2	-12.3	-12.1	-3.3
Trakarding	5.4	2.3	718.8	896.9	55669.7	1.6	1.6	0.8	12.4	12.1	5.8	-10.2	-10.0	-4.8	2.2	2.1	1.0
Weart1	10.9	6.4	964.0	1302.5	85446.5	3.5	3.8	0.6	82.8	91.3	14.2	-41.8	-46.1	-7.2	41.0	45.2	7.0
Weart2	8.4	4.9	865.5	1102.0	82942.2	2.5	3.2	0.6	44.2	57.0	11.1	-20.8	-26.9	-5.3	23.4	30.1	5.9
Weissee	3.3	2.1	710.0	771.9	74833.8	1.9	3.0	0.7	11.7	18.8	4.7	-4.1	-6.6	-1.6	7.6	12.2	3.0
Yala	1.7	2.2	715.6	690.4	55965.1	1.1	1.5	0.8	2.7	3.6	2.0	1.0	1.3	0.7	3.7	4.9	2.7

References

Arigony-Neto, J., Jaña, R., Gonzalez, I., Schneider, C., and Temme, F.: Automatic Weather Station observations at Schiaparelli Glacier, Sep 2015 - Feb 2019, PANGAEA, https://doi.org/10.1594/PANGAEA.958693, in: Arigony-Neto, J et al. (2023): Meteorological Observations at Schiaparelli Glacier Automatic Weather Station (AWSglacier), Cordillera Darwin, Chile, 2013-2019 [dataset publication series]. PANGAEA, https://doi.org/10.1594/PANGAEA.958694, 2023.

Bolton, D.: The Computation of Equivalent Potential Temperature, Monthly Weather Review, 108, 1046 – 1053, https://doi.org/10.1175/1520-0493(1980)108<1046:TCOEPT>2.0.CO;2, 1980.

Buck, A. L.: New Equations for Computing Vapor Pressure and Enhancement Factor, Journal of Applied Meteorology and Climatology, 20, 1527 – 1532, https://doi.org/10.1175/1520-0450(1981)020<1527:NEFCVP>2.0.CO;2, 1981.

Buri, P., Truffer, M., Fochesatto, J., and Aschwanden, A.: Automatic weather station data from the debris- covered Kennicott Glacier, Alaska (May-Aug 2019), https://doi.org/10.5281/zenodo.6424158, 2022.

Conrad, V.: Usual formulas of continentality and their limits of validity, Eos, Transactions American Geophysical Union, 27, 663–664, 1946.

Cuffey, K. and Paterson, W.: The Physics of Glaciers, Academic Press, ISBN 9780080919126, https://books.google.co.in/books?id=Jca2v1u1EKEC, 2010.

Galos, S. P.: Weather Station raw-data Langenferner-Felsköpfl 2012-2015, https://doi.org/10.1594/PANGAEA.902771, 2019.

Gorelick, N., Hancher, M., Dixon, M., Ilyushchenko, S., Thau, D., and Moore, R.: Google Earth Engine: Planetary-scale geospatial analysis for everyone, Remote Sensing of Environment, https://doi.org/10.1016/j.rse.2017.06.031, 2017.

ICIMOD: Meteorological data from Yala Base Camp automatic weather station, [Data set], https://doi.org/10.26066/RDS.26859, accessed: 2025-07-22, 2016.

ICIMOD and Utrecht University: Micromet station: Lirung glacier, [Data set], https://doi.org/10.26066/RDS.1972409, accessed: 2025-07-22, 2020a.

ICIMOD and Utrecht University: Micromet station: Morimoto, [Data set], https://doi.org/10.26066/RDS.1972408, accessed: 2025-07-22, 2020b.

Mandal, A., Angchuk, T., Azam, M. F., Ramanathan, A., Wagnon, P., Soheb, M., and Singh, C.: An 11-year record of wintertime snow-surface energy balance and sublimation at 4863 m asl on the Chhota Shigri Glacier moraine (western Himalaya, India), The Cryosphere, 16, 3775–3799, 2022.

Matthews, T. and Coauthors: Going to Extremes: Installing the World's Highest Weather Stations on Mount Everest, Bulletin of the American Meteorological Society, 101, E1870–E1890, https://doi.org/10.1175/BAMS-D-19-0198.1, 2020.

QGIS Development Team: QGIS Geographic Information System, Open Source Geospatial Foundation Project, http://qgis.osgeo.org, 2024.

RGI7.0-Consortium: Randolph Glacier Inventory - A Dataset of Global Glacier Outlines, Version 7.0, https://doi.org/10.5067/f6jmovy5navz, 2023.

Shea, J. M.: Regional-scale distributed modelling of glacier meteorology and melt, southern Coast Mountains, Canada, Ph.D. thesis, University of British Columbia, https://doi.org/http://dx.doi.org/10.14288/1.0069481, 2010.

Stocker-Waldhuber, M., Emprechtinger, M., and Fischer, A.: Continuous meteorological observations at weather station HEF (Hintereisferner), Ötztal Alps, Austria, in 2012, https://doi.org/10.1594/PANGAEA.809095, 2013.

Stocker-Waldhuber, M., Seiser, B., and Fischer, A.: Meteorological data Weißseespitze/Austria, 2017-10-31 to 2018-09-30, PANGAEA, https://doi.org/10.1594/PANGAEA.939824, 2022.

Strasser, U. and Marke, T.: Continuous meteorological observations at station Bella Vista in 2016, PANGAEA, https://doi.org/10.1594/PANGAEA.879211, 2017.

Tadono, T., Ishida, H., Oda, F., Naito, S., Minakawa, K., and Iwamoto, H.: Precise Global DEM Generation by ALOS PRISM, ISPRS Annals of the Photogrammetry, Remote Sensing and Spatial Information Sciences, II-4, 71–76, https://doi.org/10.5194/isprsannals-II-4-71-2014, 2014.